

Central Higgs Production at LHC from Single- P -Exchange

Samim Erhan^a, Victor T. Kim^{bc} and Peter E. Schlein^a

^aUniversity of California*, Los Angeles, California 90095, U.S.A.

^bSt. Petersburg Nuclear Physics Institute, Gatchina 188300, Russia

^cCERN, CH-1211, Geneva 23, Switzerland

Abstract

Contrary to common perceptions about systems produced in Single-Pomeron-Exchange (SPE) pp interactions, the hard diffractive process discovered at the CERN $S\bar{p}pS$ -Collider leads to dominant central production of Higgs bosons at the LHC. The rate for SPE production of Higgs bosons is calculated to be 7-9% of the total inclusive Higgs rate. In addition, an SPE measurement program of dijet events is outlined for the early days of LHC running which should answer many fundamental questions about the Pomeron structure and its effective flux factor in the proton.

Submitted to European Physical Journal C

* Supported by U.S. National Science Foundation Grant PHY-9986703

1 Introduction

A primary physics goal of the Large Hadron Collider project (LHC) is the discovery and study of the Higgs boson, whose production is expected to be mainly via the gluon–fusion process, $gg \rightarrow Higgs$. The data analysis strategy for such interactions has long been an important topic in planning for the major experiments, ATLAS and CMS. Although certain types of background are irreducible, for example $gg \rightarrow b\bar{b}$, it nonetheless seems self evident that a general reduction of hadronic activity in the final state must improve the capability for Higgs detection and isolation.

In a typical interaction in which a 120 GeV Higgs boson is produced at the LHC, a gluon participating in the fusion process has only about 1% of the 7 TeV beam momentum. Thus, about 99% of the beam energy resides in other partons which are responsible for the overall hadronic activity. An alternate approach to inclusive Higgs study is to focus on the Pomeron–Exchange class of events (also known as “diffraction”), where much of the excess beam energy is carried away by a single proton on one or both sides of the interaction. Recently, much attention has been paid to Higgs production via Double–Pomeron-Exchange [1, 2] In this paper, because the cross section is much larger, we discuss the Single–Pomeron–Exchange process (SPE) where only a single proton emerges.

$$p + p \rightarrow p + X \rightarrow p + (HY), \quad (1)$$

The final state proton and the (HY) system each recoil with more than 90% of the initial 7 TeV beam momentum. Previous discussions of this reaction are in [3, 4, 5] with cross section predictions ranging from 1% to 25% of the total Higgs cross section.

We now understand that diffractive processes occur because of the existence of colorless gluon-dominant clusters (for example, di–gluons) in the partonic sea of a proton which interact with the other beam proton. The existence of objects in a proton’s sea with most likely momentum fraction of their host proton near zero is linked to the observations starting about 40 years ago [6] of inclusively–measured final–state protons from inelastic interactions which possessed nearly all the initial beam momentum.

There is solid empirical evidence for the existence of such clusters. The UA8 Experiment [7] at the CERN $S\bar{p}pS$ –Collider observed jet production in this class of events, demonstrating the hard partonic structure of the clusters. The H1 experiment [8] at the DESY HERA ep –Collider studied γ^* interactions with rapidity gaps and demonstrated that the clusters have dominant gluon structure.

In the present paper, we show that the hard Pomeron–proton collision which creates the (HY) system in React. 1 results in the Higgs emerging in the central region of the pp center–of–mass. To calculate the cross section for React. 1, we assume effective factorization between the probabilities to find a Pomeron and its interaction with the other proton [9]:

$$\frac{d^2\sigma}{dt d\xi} = F_{\mathbb{P}/p}(t, \xi) \cdot \sigma_{\mathbb{P}p \rightarrow HY}(M_X) \quad (2)$$

where $F_{\mathbb{P}/p}(t, \xi)$ is the Pomeron flux factor in the proton, which depends on the squared 4–momentum transfer, t , to the proton and $\xi = 1 - x_p$, the Pomeron’s momentum fraction

of its host proton. $\sigma_{\mathbb{P}p \rightarrow HY}(M_X)$ is the Higgs cross section, where M_X is the invariant-mass of the Pomeron-proton (or HY) system. To good approximation, $M_X^2 = \xi s$, where s is the total squared c.m. energy. We discuss the limitations of the cross section calculation and outline how a series of measurements can be made at the LHC to test the fundamental aspects of Pomeron-exchange reactions.

Section 2 contains a discussion of the kinematics of React. 1 and shows what can be learned from the data without prior knowledge of the Pomeron flux factor and its structure function. Section 3 contains the calculation of the Pomeron-proton cross section in Eq. 2 and explains how the Pomeron structure function can be determined in hadronic interactions. Section 4 introduces the Pomeron flux factor and how it is determined empirically. Section 5 then uses it to calculate the total cross section for React. 1. Discussion and conclusions are in Sect. 6.

2 Kinematics

In the pp center-of-mass (the laboratory system), the mass of the Higgs, M_H , and its Feynman- x , x_H^{pp} , can be expressed in terms of the two interacting gluons' momentum fractions of their host protons, ξ_1 and ξ_2 , respectively:

$$M_H^2 = \xi_1 \xi_2 s \quad (3)$$

$$x_H^{pp} = \xi_1 - \xi_2, \quad (4)$$

where $s = (14 \text{ TeV})^2$ at the LHC. If ξ_1 is assumed to arise from an intermediate di-gluon state (the Pomeron), then:

$$\xi_1 = \beta \xi \quad (5)$$

where $\xi = 1 - x_p$ is the Pomeron's momentum fraction of its host proton and β is the gluon's momentum fraction in the Pomeron. Eqs. 3, 4 and 5 are combined to give:

$$x_H^{pp} = \beta \xi - \frac{M_H^2}{\beta \xi s} \quad (6)$$

Figure 1 displays Eq. 6 for React. 1. We see that, for fixed M_X (and therefore also ξ), the longitudinal Higgs momentum in the laboratory is uniquely related to a value of β . In other words, the observed distribution of $P_{||}$ reflects the Pomeron structure function. The precise relationship also depends on the gluon structure function of the proton, as discussed in the next section. To sum over all possible M_X values, knowledge of the Pomeron flux factor in the proton is needed, as discussed in Sect. 4.

We also note that, for fixed M_X and for the maximum value, $\beta = 1$, $P_{||}$ has a maximum value in the laboratory. Fig. 1 also shows that the centrality of Higgs production can be influenced by an appropriate selection of x_p . Furthermore, for $P_{||} = 0$, and if we require $\xi < 0.1$ (in order to have relatively clean Pomeron exchange), there is a minimum value of β that is sampled; it is $\beta \sim 0.1$ for $M_H = 120 \text{ GeV}$ at the LHC and increases either with larger mass or smaller s .

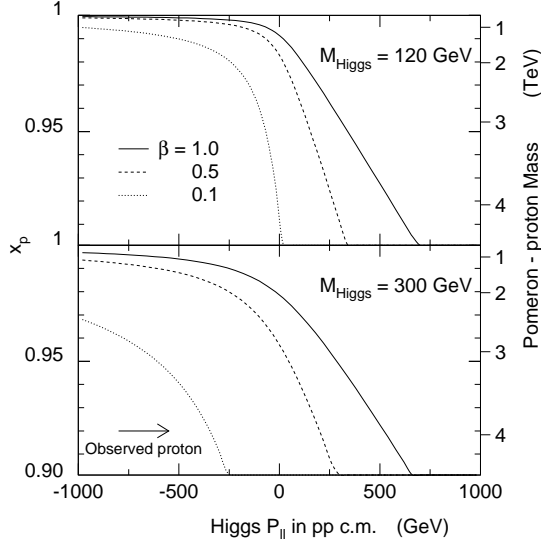


Figure 1: *Higgs SPE kinematics at LHC for $M_H = 120$ and 300 GeV,,: Longitudinal Higgs momentum in the laboratory vs. observed proton Feynman- x_p for three values of a gluon's momentum fraction, β , of its host Pomeron. Positive Higgs' momentum corresponds to the direction of the observed final state proton.*

3 Higgs cross section in Pomeron–proton collisions

The basis of all cross sections given in this paper is the cross section for gluon-gluon fusion into Higgs boson at a gluon-gluon mass-squared, \hat{s} , which can be written as:

$$\sigma_{gg \rightarrow H}(M_H, \hat{s}) = K_{HO} \cdot \sigma_{LO} \cdot [\hat{s} \cdot \delta(\hat{s} - M_H^2)] \quad (7)$$

where the leading order Higgs cross section is [10]:

$$\sigma_{LO} = \frac{G_F \alpha_S^2}{288 \sqrt{2} \pi} \left| \frac{3}{4} \sum_q A_q(M_H/M_q) \right|^2 \quad (8)$$

A_q is the matrix element for the $gg \rightarrow H$ process, dominantly via a q -quark loop in leading order. The last factor in Eq. 7 is the zero-width approximation for the Higgs boson which, for $M_H \leq 400$ GeV, is known to be a good approximation. The factor, K_{HO} , accounts for higher-order perturbative QCD corrections and is taken in the next-to-next-to-leading order [11]: $K_{HO} = K_{NNLO} \simeq 2$ (3) for LHC (Tevatron) energy.

In the Pomeron–proton center-of-mass system with fixed invariant mass, M_X , we write the cross section for inclusive Higgs boson production in terms of the standard gluon distribution function of the proton [12] taken at the scale $Q^2 = M_H^2$, the gluon distribution function of the Pomeron (see below) and the cross section for $gg \rightarrow H$ using Eq. 7:

$$\sigma_{\mathbb{P}p \rightarrow H}(M_H, M_X) = C_g \cdot \int_0^1 \int_0^1 F_{g/p}(\xi_p) \cdot F_{g/\mathbb{P}}(\beta) \cdot \sigma_{gg \rightarrow H}(M_H, \hat{s}) \, d\beta \, d\xi_p \quad (9)$$

where:

$$\hat{s} = \beta \xi_p M_X^2 \quad (10)$$

is the squared invariant mass of the 2-gluon system and β and ξ_p are the gluon momentum fractions of their host Pomeron and proton, respectively. $C_g = 0.8$ is the estimated fraction of the Pomeron momentum that resides in the gluons [8].

Equation 10 and the δ -function in Eq. 7 allow Eq. 9 to be simplified to:

$$\sigma_{\mathbb{P}p \rightarrow H}(M_H, M_X) = C_g \cdot K_{HO} \cdot \sigma_{LO} \cdot \int_{\tau}^1 F_{g/p}\left(\frac{\tau}{\beta}\right) \cdot F_{g/\mathbb{P}}(\beta) \cdot \frac{\tau}{\beta} d\beta \quad (11)$$

where: $\tau = (M_H/M_X)^2$.

The Feynman- x of a produced Higgs boson in the Pomeron-proton center-of-mass is given in terms of the gluon momentum fractions as:

$$x_H = \beta - \xi_p = \beta - \tau/\beta \quad (12)$$

Equation 12 allows us to write the differential cross section in x_H as:

$$\frac{d\sigma_{\mathbb{P}p \rightarrow H}(M_H, M_X)}{dx_H} = C_g \cdot K_{HO} \cdot \sigma_{LO} \cdot F_{g/p}\left(\frac{\tau}{\beta}\right) \cdot F_{g/\mathbb{P}}(\beta) \cdot \frac{\tau}{\beta} \cdot \left[1 + \frac{x_H}{(x_H^2 + 4\tau)^{1/2}}\right] \quad (13)$$

and where $\beta = 0.5 \left[x_H + (x_H^2 + 4\tau)^{1/2} \right]$.

We evaluate these equations for several possible Pomeron structure functions [13]. Figure 2, reproduced from the original UA8 dijet paper [7], shows their experimental distribution of Feynman- x for the dijet system in the Pomeron-proton center-of-mass, “ $x(2\text{-jet})$ ”. Almost all dijet systems travel in the Pomeron hemisphere¹. As pointed out in [13], such an observation means that the Pomeron structure is much harder than the proton structure. The two curves in Fig. 2(a) show the shapes of the expected $x(2\text{-jet})$ distributions (with arbitrary normalization) for two examples of possible Pomeron structure functions:

$$\text{“Soft”} : \quad \beta F_{g/\mathbb{P}}(\beta) = 6(1 - \beta)^5 \quad (14)$$

$$\text{“Hard”} : \quad \beta F_{g/\mathbb{P}}(\beta) = 6\beta(1 - \beta)^1 \quad (15)$$

For both curves in Fig. 2(a), PYTHIA [14] was used to calculate hadronization effects and initial-state and final-state radiation; this was followed by a full simulation of the UA2 calorimeter [15] which detected the jets with $E_T > 8$ GeV. This method of comparing “smeared theoretical predictions” with observations is a reliable way to compare theory with experiment (see also comments in [16]). About 30% of the observed $x(2\text{-jet})$ distribution is harder than the hard function of Eq. 15. UA8 therefore called the Pomeron structure “Super-Hard” [7]. To parametrize this component, they assumed that the entire momentum of the Pomeron participated in the hard scattering as a gluon. In that case, $\beta = 1$ and $x(2\text{-jet}) = 1 - \xi_p$ is the scattered parton distribution before hadronization and

¹There is no major acceptance loss in the first part of the proton hemisphere.

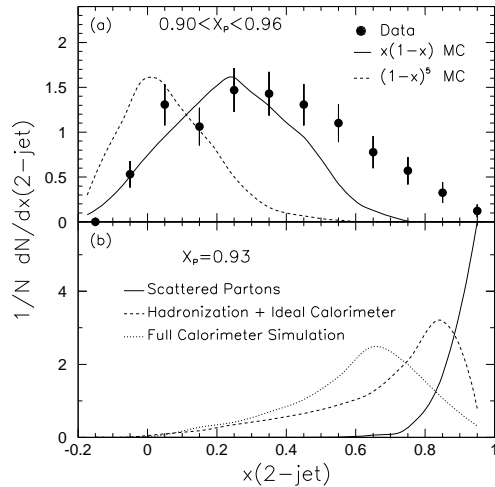


Figure 2: UA8 results [7] in the Pomeron-proton center-of-mass: (a) Observed Feynman- x_F distribution of dijet systems. The positive x -axis is in the Pomeron hemisphere; (b) Results of $x(2\text{-jet})$ calculation in PYTHIA, assuming the entire momentum of the Pomeron participates in the hard scattering as a gluon. See discussion in text.

detector effects; shown as the solid curve in Fig. 2(b)². The dotted curve shows the effects of hadronization and full detector simulation. When added to the solid (Hard) curve in Fig. 2(a), the dotted curve accounts nicely for the excess of events at large $x(2\text{-jet})$ in the experimental distribution.

We therefore assume a Pomeron structure function to be the following weighted sum of a gluonic Hard structure, and a smeared δ -function³. For the latter, we use the function suggested by Alvero et al. [18]:

$$\text{“Hard + SuperHard”} : \quad \beta F_{g/P}(\beta) = 0.7 \left[6 \beta (1 - \beta) \right] + 0.3 \left[19.8 \beta^8 (1 - \beta)^{0.3} \right] \quad (16)$$

The essential property of this type of function required by the UA8, H1 and ZEUS data [7, 8, 19] is that it extends to $\beta = 1$. The details of its shape do not greatly influence the Higgs predictions presented here. For all three types of Pomeron structure, their integrals are unity; in other words, a momentum sum rule is assumed to be satisfied and the constituents of the Pomeron carry all its momentum. The momentum sum rule is discussed further in Sect. 6. The evaluation of Eq. 13 using the Pomeron structure functions in Eqs. 14, 15 and 16 leads to the curves shown in Fig. 3 for fixed $M_X = 3$ TeV and $M_H = 120$ GeV.

Following the arguments of [13], plots of experimental distributions as in Figs. 2 and 3 directly compare the relative hardness of the Pomeron structure with the proton structure.

²We note that because the di-gluon mass is not unique for jet formation, the solid curve in Fig. 2(b) displays the features of the gluon component of the proton structure function

³For discussion of a δ -function component in the Pomeron, see [17].

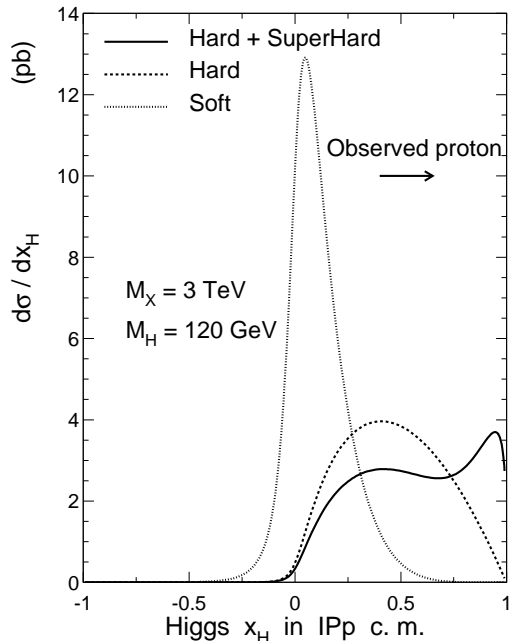


Figure 3: *Differential cross section vs. Feynman- x_F of a 120 GeV mass Higgs boson in the Pomeron-proton center-of-mass in React. 1, calculated assuming $M_X = 3$ TeV and the three Pomeron structure functions given in Eqs. 14, 15 and 16. Positive x_H is in the observed proton direction.*

With more common final states at the LHC, such as $t\bar{t}$, $b\bar{b}$ and dijets it will in practice be possible to perform high statistics determination of the Pomeron structure function as a function of Q^2 .

Of course, following the arguments of Sect. 2, it is possible to also obtain the Pomeron structure function from the longitudinal momentum distributions in the laboratory using data at fixed $x_p = 1 - \xi$ values. The results from Eq. 13 and Fig. 3 can be transformed to the laboratory frame using the Lorentz transformation:

$$\gamma = \frac{1 + \xi}{2\sqrt{\xi}}. \quad (17)$$

This leads to the distributions of longitudinal Higgs momentum in the laboratory shown in Fig. 4. Figure 4 also explicitly shows that, by selecting recoil proton momentum ranges using the Roman pots, the mean Higgs longitudinal momentum can be “tuned”.

4 The Pomeron flux-factor

In order to relate our calculated $\sigma_{Pp \rightarrow HY}$ to observed cross sections, the probability to find a Pomeron in the proton at fixed ξ and t must be included. In this section we

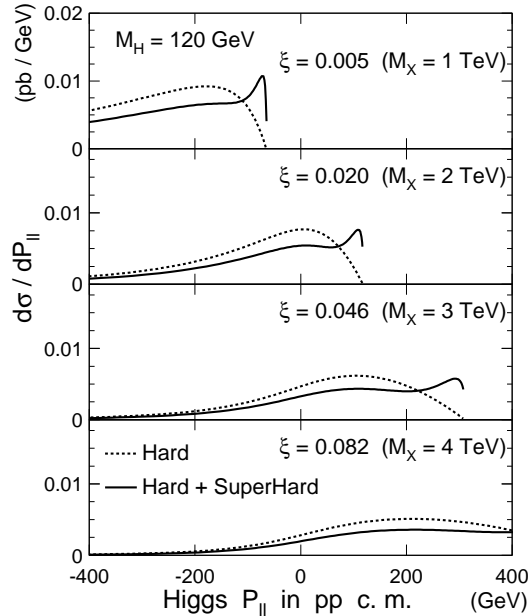


Figure 4: *Higgs momentum along the beam axis in the laboratory frame (positive values are in the observed proton direction) for four values of M_X and ξ . $M_H = 120$ GeV. The upper limit in Higgs momentum for each set of curves corresponds to $\beta = 1$, as seen in Fig. 1.*

summarize our present empirical knowledge of the Pomeron flux factor and, in the process, also point out its limitations and where new measurements will help.

The Pomeron flux factor has been determined for hadronic interactions by using the inclusive inelastic diffractive process:

$$p + p \rightarrow p + X \quad (18)$$

and its corresponding $\bar{p}p$ reaction. Such analyses are based on the assumption that the observed cross sections are the product of two factors, the Pomeron flux factor and the relevant Pomeron–proton total cross section, $\sigma_{\mathbb{P}p}(M_X)$, at invariant mass, M_X . For React. 18, the measured cross section is written as:

$$\frac{d^2\sigma_{pp}^{\text{dif}}}{dt d\xi} = F_{\mathbb{P}/p}(t, \xi) \cdot \sigma_{\mathbb{P}p \rightarrow X}(M_X). \quad (19)$$

Refs. [21, 22] contain the results of fitting Eq. 19 to all available data on React. 18 from the CERN Intersecting Storage Rings [23] to the CERN $S\bar{p}pS$ –Collider [21, 24], covering the energy range, $\sqrt{s} = 23$ GeV to 630 GeV and over the extended ranges, $|t| < 2$ GeV² and $\xi < 0.09$.

The self-consistent set of fits reported in [21, 22] are equivalently important as those made to the diffractive DIS events by the H1 [8] and ZEUS [20] collaborations. The fits

show that factorization between Pomeron flux and Pomeron cross section, as embodied in Eq. 19, describes all available data at low ξ . This is all the more remarkable, since the empirical flux factors differ in ep and pp interactions because of their different effective Pomeron trajectory intercepts [9];

All fits in [21, 22] use the following standard Regge form for the flux factor [25] and the Pomeron–proton total cross section⁴. Except for the Pomeron Regge trajectory which we discuss below, the fitted parameters in [21] are shown:

$$F_{\mathbb{P}/p}(t, \xi) = K \cdot |F_1(t)|^2 \cdot e^{(1.1 \pm 0.2)t} \cdot \xi^{1-2\alpha(t)} \quad (20)$$

$$K \sigma_{\mathbb{P}p}^{\text{tot}}(s') = (0.72 \pm 0.10) \cdot [(s')^{0.10} + (4.0 \pm 0.6)(s')^{-0.32}] \text{ mb GeV}^{-2}. \quad (21)$$

where $s' = M_X^2$. Equation 19 shows that, in performing fits to data, the scale factor, K , of the flux factor can not be separated from a scale factor, σ_0 , of the cross section. Therefore, the value of the fitted product, $K\sigma_0$, is given in Eq. 21. With the exponents⁵ of $s' = \xi s$ fixed at 0.10 and -0.32, respectively, $K\sigma_{\mathbb{P}p}^{\text{tot}}(s')$ requires the presence of both Pomeron exchange and Reggeon exchange terms. With $|F_1(t)|^2$ in Eq. 20 set equal to the Donnachie–Landshoff [25] form factor⁶, the additional exponential factor is required.

Finally, concerning $\alpha(t)$, Ref. [22] demonstrated that, contrary to Regge theory, in which Regge poles are fixed, the data on React. 18 demonstrate that $\alpha(t)$ is an “effective trajectory”. That is, it changes with interaction energy. Its intercept at $t = 0$ decreases and its slope flattens as energy increases. As predicted by Kaidalov et al. [28], the reason for this is likely the result of complications due to multi–Pomeron–exchange effects. In this connection, we note that the highest energy at which a fitted effective trajectory has been obtained [22] is at $\sqrt{s} = 630$ GeV:

$$\alpha(t) = 1 + \epsilon + \alpha' t + \alpha'' t^2 = 1.035 + 0.165 t + 0.059 t^2 \quad (22)$$

It is shown in [22] that this effective trajectory is also compatible with the published function which was fit to the CDF data [29] at $\sqrt{s} = 2$ TeV.

Since we have no information as to the effective values of $\alpha(t)$ at the LHC energy, all cross section calculations reported in this paper are given for two values of the intercept, $\alpha(0) = 1.035$ and 1.000. The latter value was suggested by Schuler & Sjöstrand [30] for use at ultra–high energies. Since all evidence shows that the effective Pomeron trajectory intercept decreases with increasing energy, it seems like a reasonable choice to make. In any case, our results do not depend greatly on which of these two values is used.

Figure 5(a) shows the ξ –dependence of the flux factor of Eq. 20 integrated over all t . The choice of the K value assumed is perhaps the weakest aspect of the predictions, for there is neither a measurement nor a reliable prediction for K . The best we can do is use the value of K which Donnachie & Landshoff [31] extracted from elastic-scattering

⁴Eq. 21 is the same function typically used to fit the s –dependence of other total cross sections [26, 27].

⁵In this formula, “ s' ” stands for “ s'/s_0 ”, where $s_0 = 1$ GeV².

⁶ $F_1(t) = \frac{4m_p^2 - 2.8t}{4m_p^2 - t} \cdot \frac{1}{(1-t/0.71)^2}$

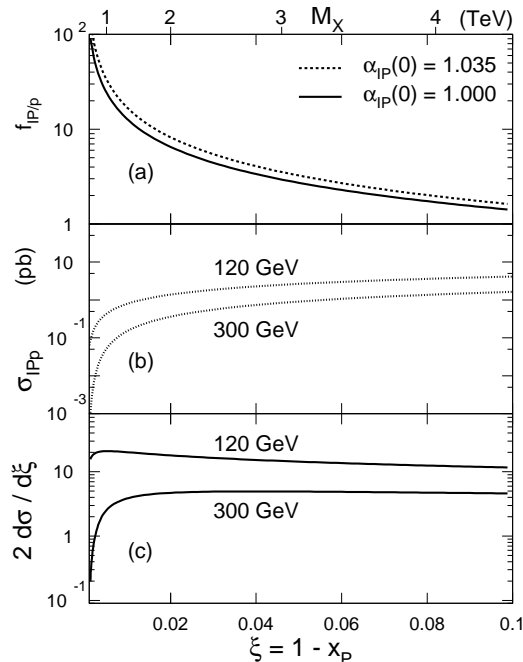


Figure 5: Dependence on ξ and M_X of: (a) Flux factor in Eq. 20 integrated over all t , using the Pomeron effective trajectory in Eq. 22 with $\epsilon = 0.035$, and then 0.0. $K = 0.78 \text{ GeV}^{-2}$ is assumed. (b) The Pomeron–proton to Higgs cross section, calculated for the two indicated Higgs masses using Eq. 11 and the Hard + SuperHard Pomeron structure function. (c) Cross section for React. 1 (the product of the solid curve in (a) and each curve in (b)), multiplied by a factor of 2 to account for final state proton detection in both arms.

data, namely $K = 0.78 \text{ GeV}^{-2}$, although given the observed s -dependence of the effective Pomeron trajectory discussed above, we see no reason why this value of K should also apply precisely to inelastic diffraction where multi-Pomeron-exchange effects may be different. We therefore regard it as an approximation. However, we discuss tests of this issue in Sect. 6.

5 Total Higgs cross section via SPE

The total Higgs cross section via the SPE mechanism can now be calculated. Fig. 5(b) shows $\sigma_{\mathbb{P}p \rightarrow H}(M_H, M_X)$ plotted vs. M_X and ξ for two values of M_H . The product of the flux factor and $\sigma_{\mathbb{P}p \rightarrow H}(M_H, M_X)$ is the t -integrated version of Eq. 2 and is shown in Fig. 5(c), multiplied by a factor of 2 to account for the use of Roman pot spectrometers in both arms. $\alpha_{\mathbb{P}}(0) = 1.0$ is assumed for both parts (b) and (c) of Fig. 5. Finally, Fig. 6 shows the ξ -integral of the differential cross section in Fig. 5 vs. Higgs mass. At LHC, SPE Higgs production (with recoil protons measured in *either* arm) is between 7% and

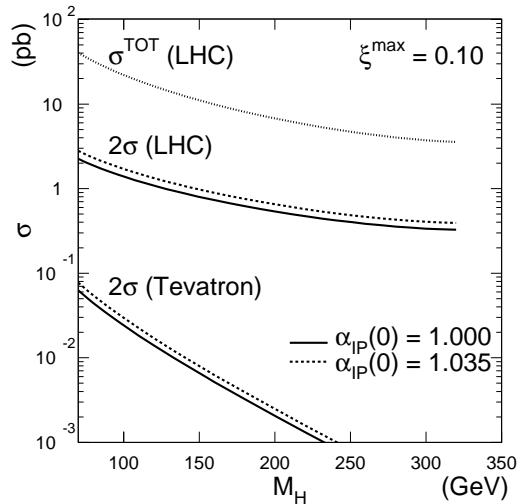


Figure 6: Upper curve is the total inclusive Higgs boson cross section vs. Higgs mass, calculated for the gluon–gluon fusion process. Central curves are the LHC cross section of Fig. 5(c) integrated over $\xi < 0.1$, for the two indicated values of $\alpha_P(0)$. The lower curves are the same, but for the Tevatron.

9% of the total Higgs cross section, depending on M_H .

The Higgs longitudinal momentum in the laboratory integrated over all M_X is shown in Fig. 7. This figure gives us global views of the centrality of Higgs production integrated over all ξ in the range: $0 < \xi < 0.1$. The distributions do not depend greatly on the detailed shape of the Pomeron structure function at large β .

6 Discussion & Conclusions

We have drawn attention to the method used by the UA8 Collaboration [7, 13] to determine the Pomeron structure function. The longitudinal momentum distribution of the system produced via hard scattering reflects the relative hardness of the Pomeron and proton structure functions. The analysis can be carried out either in the Pomeron proton c.m. or in the laboratory although, in the later case, it must be done at fixed value of $x_p = 1 - \xi$. Progress in further understanding the Pomeron will be possible at the LHC by making high–statistics measurements of more common final states than those with Higgs bosons, for example dijets, $t\bar{t}$ or $b\bar{b}$.

One of the parameters most poorly understood is the normalization, K , of the Pomeron flux factor in the proton. To further understand this issue, the following ratio can be measured over a large range of t and ξ :

$$\mathcal{R} = \frac{\Delta\sigma_{pp \rightarrow p(\text{dijet}+Y)}}{\Delta\sigma_{pp \rightarrow p(X)}} \quad (23)$$

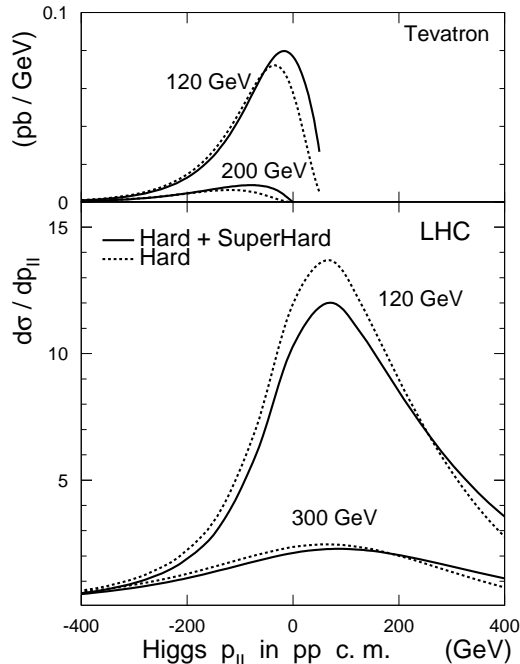


Figure 7: *Differential cross sections at LHC and Tevatron for React. 1 vs. $P_{||}$ of the Higgs in the laboratory frame for the two indicated Higgs masses and two assumed Pomeron structure functions.*

If factorization between flux factor and $\mathbb{P}p$ cross sections remains valid, the ratio, \mathcal{R} , will be found to be independent of t at fixed ξ . If that is the case, then the flux factor cancels out of the ratio and we have:

$$\mathcal{R} = \frac{K \Delta \sigma_{\mathbb{P}p \rightarrow (\text{dijet}+Y)}}{K \Delta \sigma_{\mathbb{P}p \rightarrow (X)}} \quad (24)$$

Numerator and denominator of Eq. 24 have been multiplied by K , because the denominator is then a measurable quantity (by fitting Eqs. 20, 21 and 22 to the data). The numerator of the right-hand side of Eq. 24 can then be extracted and compared with the calculated dijet cross section.

This comparison allows K to be determined although, strictly speaking, a possible violation of the momentum sum rule in the calculated dijet cross section means that the quantity measured is actually “ fK ”, where $f < 1.0$ if the sum rule is violated. UA8 carried out this procedure [32] with their limited statistics dijet data. For a pure gluonic Pomeron, they found:

$$fK = 0.38 \pm 0.13 \quad (25)$$

We have already pointed out that the Donnachie-Landshoff value, $K = 0.78 \text{ GeV}^{-2}$ which was extracted from elastic scattering data may not be precisely applicable to inelastic diffractive data, because of different multi-Pomeron-exchange effects. Thus, if the

momentum sum rule is valid, Eq. 25 is a measure of K for inelastic diffraction. On the other hand, it could reflect a product of the two effects. In either case, taking Eq. 25 at face value would mean that all cross sections presented in this paper are overestimated by a factor of 2.0 ± 0.7 . Studying fK obtained in this way for different final states and over a wide range of kinematics should shed additional light on its correct interpretation.

In conclusion, we have shown that Hard Diffraction Scattering with Single-Pomeron-Exchange leads to Higgs production dominantly in the central region. The extent to which the decrease in hadronic activity characteristic of such reactions will actually improve Higgs identification and isolation is best shown with the aid of full event simulation using the PYTHIA software package [33]. Such studies are underway. We have also briefly outlined an initial program for SPE production of dijet events which should lead to major improvements in our knowledge of the Pomeron structure and its flux factor in the proton.

Acknowledgements

We are greatly indebted to the CERN laboratory for their continued hospitality. This analysis work was carried out at the CERN site, as was the UA8 experiment whose results provided much of the underlying inspiration. One of us (V.T.K.) is supported in part by the Russian Foundation for Basic Research (RFBR), the INTAS and the U.S. N.S.F.

References

- [1] A. Schäfer, O. Nachtmann and R. Schöpf, Phys. Lett. B 249 (1990) 331;
A. Bialas and P.V. Landshoff, Phys. Lett. B 256 (1991) 540.
- [2] See, for example: V.A. Khoze, A.D. Martin and M.G. Ryskin, Eur. Phys. J. C 26 (2002) 229, hep-ph/0207313;
A. De Roeck and C. Royon, Acta Phys. Polon. B 33 (2002) 3491, hep-ph/0209171;
and references therein.
- [3] D. Graudenz and G. Veneziano, Phys. Lett. B 365 (1996) 302, hep-ph/9508401.
- [4] M. Heyssler, Z. Kunszt and W. J. Stirling, Phys. Lett. B 406 (1997) 95, hep-ph/9702286.
- [5] R. Enberg, G. Ingelman, A. Kissavos and N. Timneanu, Phys. Rev. Lett. 89 (2002) 081801, hep-ph/0203267.
- [6] See, for example: E. Gellert et al., Phys. Rev. Letters 17 (1966) 884 and references therein of earlier counter experiments.
- [7] A. Brandt et al. [UA8 Collaboration], Phys. Lett. B 297 (1992) 417.
- [8] C. Adloff et al. [H1 Collaboration], Zeit. f. Physik C 76 (1997) 613.
- [9] S. Erhan & P. Schlein, “A new $\gamma^*p/\bar{p}p$ factorization test in diffraction, valid below $Q^2 \sim 6 \text{ GeV}^2$ ”, hep-ph/0301277.
- [10] H. M. Georgi, S. L. Glashow, M. E. Machacek and D. V. Nanopoulos, Phys. Rev. Lett. 40 (1978) 692.
- [11] S. Catani, D. de Florian and M. Grazzini, JHEP 0105 (2001) 025, hep-ph/0102227;
JHEP 0307 (2003) 028, hep-ph/0306211;
R. V. Harlander and W. B. Kilgore, Phys. Rev. D 64 (2001) 013015, hep-ph/0102241;
Phys. Rev. Lett. 88 (2002) 201801, hep-ph/0201206;
C. Anastasiou and K. Melnikov, Nucl. Phys. B 646 (2002) 220, hep-ph/0207004.
- [12] H. L. Lai *et al.* [CTEQ Collaboration], Eur. Phys. J. C 12 (2000) 375, hep-ph/9903282.
- [13] G. Ingelman and P. E. Schlein, Phys. Lett. B 152 (1985) 256.
- [14] See [7] for the detailed references to the modified PYTHIA 4.8 and JETSET 6.3 programs used. See also: P. Bruni and G. Ingelman, DESY 93-187.
- [15] A. Beer et al. [UA2 Collaboration], Nucl. Instrum. Methods A 224 (1984) 360;
J. Alitti et al., Phys. Lett. B 257 (1991) 232.

- [16] J. C. Collins, J. Huston, J. Pumplin, H. Weerts and J. J. Whitmore, Phys. Rev. D 51 (1995) 3182, hep-ph/9406255.
- [17] J. C. Collins, L. Frankfurt and M. Strikman, Phys. Lett. B 307 (1993) 161, hep-ph/9212212.
- [18] L. Alvero, J.C. Collins, J. Terron and J. J. Whitmore, Phys. Rev. D 59 (1999) 074022.
- [19] M. Derrick et al. [ZEUS Collaboration] Phys. Lett. B 356 (1995) 129.
- [20] I. Breitweg et al. [ZEUS Collaboration] Eur. Phys. J. C 6 (1999) 43.
- [21] A. Brandt et al. [UA8 Collaboration], Nucl. Phys. B 514 (1998) 3, hep-ex/9710004.
- [22] S. Erhan and P. Schlein, Phys. Lett. B 481 (2000) 177, hep-ex/9909035.
- [23] M. G. Albrow et al., Nucl. Phys. B54 (1973) 6; Nucl. Phys. B72 (1974) 376; Nucl. Phys. B 108 (1976) 1;
J. C. M. Armitage et al., Nucl. Phys. B 194 (1982) 365.
- [24] M. Bozzo et al. [UA4 Collaboration], Phys. Lett. B 136 (1984) 217;
D. Bernard et al., Phys. Lett. B 186 (1987) 227.
- [25] A. Donnachie and P. V. Landshoff, Nucl. Phys. B 303 (1988) 634.
- [26] R. J. M. Covolan, J. Montanha and K. Goulianos, Phys. Lett. B 389 (1996) 176.
- [27] J. R. Cudell, K. Kang and S. K. Kim, Phys. Lett. B 395 (1997) 311.
- [28] A. B. Kaidalov, L. A. Ponomarov, K. A. Ter-Martirosyan, Sov. Jour. Nucl. Phys. 44 (1986) 468.
- [29] F. Abe et al. [CDF Collaboration], Phys. Rev. D 50 (1994) 5535.
- [30] G. Schuler & T. Sjöstrand, Phys. Rev. D 49 (1994) 2257.
- [31] A. Donnachie and P. V. Landshoff, Nucl. Phys. B 231 (1984) 189; Nucl. Phys. B 244 (1984) 322; Nucl. Phys. B 267 (1986) 690.
- [32] A. Brandt et al. [UA8 Collaboration], Phys. Lett. B 421 (1998) 395, hep-ex/9709015.
- [33] T. Sjöstrand et. al., "PYTHIA 6.3 Physics & Manual", LU TP 03-38, hep-ph/0308153.